Transition between Internal Transport Barriers with Different Temperature-Profile Curvatures in JT-60U Tokamak Plasmas

K. Ida,[1] Y. Sakamoto,[2] H. Takenaga,[2] N. Oyama,[2] K. Itoh,[1] M. Yoshinuma,[1] S. Inagaki,[1,*] T. Kobuchi,[1,†] A. Isayama,[2] T. Suzuki,[2] T. Fujita,[2] G. Matsunaga,[2] Y. Koide,[2] M. Yoshida,[2] S. Ide,[2] Y. Kamada,[2] and JT-60 team

[1]*National Institute for Fusion Sciences, Toki, Gifu 509-5292, Japan*
[2]*Japan Atomic Energy Agency, Naka, Ibaraki-ken, 311-0193, Japan*

(Received 20 June 2007; revised manuscript received 1 March 2008; published 31 July 2008)

A spontaneous transition phenomena between two states of a plasma with an internal transport barrier (ITB) is observed in the steady-state phase of the magnetic shear in the negative magnetic shear plasma in the JT-60U tokamak. These two ITB states are characterized by different profiles of the second radial derivative of the ion temperature inside the ITB region (one has a weak concave shape and the other has a strong convex shape) and by different degrees of sharpness of the interfaces between the L mode and the ITB region, which is determined by the turbulence penetration into the ITB region.

DOI: 10.1103/PhysRevLett.101.055003 PACS numbers: 52.55.Fa, 52.25.Fi, 52.50.Gj

The transition from the low-confinement phase (L mode) to the high confinement phase (H mode) has been widely studied near the plasma edge in many toroidal plasmas [1–3]. Associated with the transition, the radial electric field (E_r) shear appears, and the curvatures of the temperature profiles (the second derivative of temperature profiles) change from weak positive to strong negative along with an increase of the temperature gradient (the first derivative of temperature profiles). The curvature difference is due to the characteristics of transport with (H mode) and without (L mode) the suppression of turbulence due to the $E_r \times B$ shear [4]. The fast change in E_r (less than a millisecond) triggers a first-order transition such as the onset of the H mode. However, because of the short equipartition time between the E_r and the T_i gradient, they change simultaneously in the second-order transition [5], where the importance of self-consistent transport has been pointed out theoretically by Taylor [6]. The curvature of the temperature inside the internal transport barriers (ITBs) [7–10], where a large temperature gradient is observed in the interior plasma, has not been studied quantitatively, in spite of its importance in the transport. Although a wide variety of shapes (parabolic-shaped, box-shaped) of ITBs with different curvatures as well as different magnitudes of temperature gradient are observed, the variety has been attributed mainly to the differences in the radial profile of the magnetic shear [11]. The radial profile of ion temperature T_i has been fitted by arbitrary function (linear interpolation [12] or modified hyperbolic tangent for box-shaped ITBs), and no study of internal radial structure of ITBs has been reported because of poor spatial resolutions of the conventional charge exchange spectroscopy (CXS). In this Letter, the internal structure of ITBs (the curvature of T_i) measured with modulation CXS is presented, and the spontaneous transition of internal radial structure of ITBs and a possible physics mechanism responsible for the transition are discussed. Here the T_i profiles inside the ITB are discussed, because the transition in this experiment is much slower than the E_r-T_i gradient equipartition time scale.

Spontaneous transition between the two ITB states is observed during the steady-state phase of the current profile with a constant heating power ($P_{\rm nbi} = 7.5$ MW and $P_{\rm ech} = 3$ MW for $t > 5.05$ s) well after the plasma current reaches a constant value ($B = 3.75$ T, $a = 0.8$ m, $\kappa = 1.65$, and $I_p = 1$ MA for $t > 4.75$ s). The curvature of the T_i profile is measured with the 31-channel modulation system [13], in which there are two operation modes: One is a sweeping mode which gives 310 spatial data points with the time resolution of 50 ms, and the other is a fixed mode which gives 31 spatial data points with the time resolution of 5 ms. These two ITB states are characterized by different curvatures of T_i as seen in the temperature profiles at $t = 6.04$–6.09 s and $t = 6.24$–6.29 s in Fig. 1(a). The change in curvature of the temperature profile is observed in both T_i and the electron temperature measured with electron cyclotron emission (ECE). The measurements of T_i profiles have enough accuracy to discuss the magnitude of the curvature, while the ECE measurements have not enough spatial channels to discuss the sign of the curvature [Fig. 1(b)]. Clear differences in the curvatures of T_i profiles between these two time slices are observed in the ITB region ($0.53 < \rho < 0.65$). On the other hand, T_i outside the ITB region is identical within the error bar between these two states. The change in the curvature of the temperature profile is relatively fast compared with the time scale of the current profile and, hence, the magnetic shear or the minimum q location. In fact, the safety factor q profiles measured with motional stark effect spectroscopy are identical within the error bar between the two ITB states as seen in Fig. 1(c). For both ITB states, the ITB region appears near the minimum q location ($q_{\rm min} = 3.3$). The error bars of T_e are 10% in absolute values and 2% in the relative change in time. The uncertainty of mapping to ρ among T_i, T_e, and q profiles is 0.01–0.02.

 © 2008 The American Physical Society

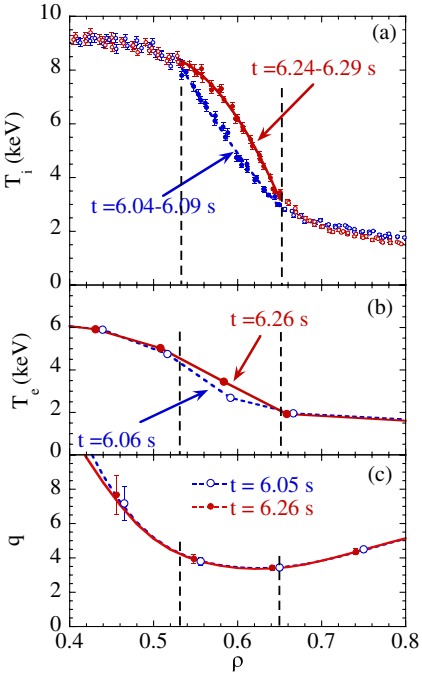

FIG. 1 (color online). Radial profiles of (a) ion temperature, (b) electron temperature, and safety factor in the plasma with concave curvature ($t = 6.06$ s) and with convex curvature ($t = 6.26$ s). The polynomial fitting curves of the ion temperature profiles inside the ITB region are also plotted. The dashed lines represent the locations of the shoulder and the foot of the ITBs, respectively.

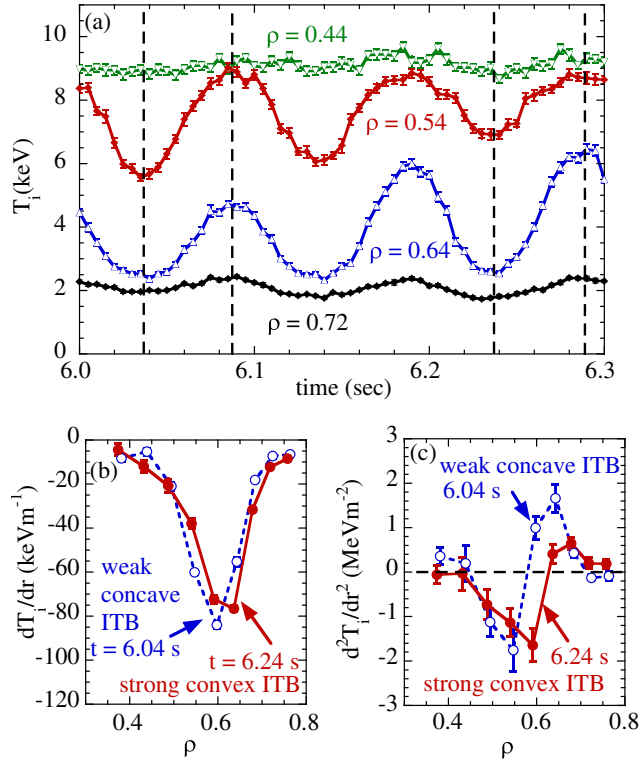

FIG. 2 (color online). (a) Time evolution of ion temperature with spatial modulation and radial profiles of the (b) first and (c) second derivative of ion temperature.

In general, the curvature of the T_i profile near the foot point is positive, while it becomes negative near the shoulder of the ITB. Therefore, the curvature of T_i should be evaluated at different radii in the ITB region to discuss the magnitude of the curvature more precisely. The first and second radial derivatives of T_i can be derived from the modulation component of the T_i measured using the Fourier series expansion technique [13]. The error bars of the first and second derivatives of T_i are evaluated from the error bars of each $T_i \sim 0.15$ keV, which is only 2% of the T_i because of the high throughput of the spectrometer of $F/2.8$ and is much smaller than the typical error bars of T_i (5%–10%) measured with conventional charge exchange spectroscopy ($F > 5$). The error bars of the third radial derivative of T_i are too large to discuss its radial structure.

Figure 2(a) shows the time evolution of T_i near the ITB shoulder ($\rho = 0.54$) and near the foot point ($\rho = 0.64$). The higher harmonic component of the time evolution (for example, observed at $\rho = 0.54$ and $\rho = 0.64$ for $t =$ 6.0–6.1 s) clearly indicates the existence of a significant second derivative of T_i profile. The radial profiles of the first and second derivatives evaluated from the time evolution of T_i profiles are plotted in Fig. 2(b) and 2(c), respectively. The maximum T_i gradient $|\partial T_i/\partial r|$ at the ITB is 80 keV/m in both of these ITBs. Although the location of the maximum gradient in the ITB region shifts outward at $t = 6.24$ s by a $\delta\rho$ of 0.02, the location of the foot point ($\rho = 0.72$) is almost unchanged. There are clear differences in the second radial derivative of T_i as seen in Fig. 2(c). The radial profiles of the second derivative have two peaks: a negative peak in the inner half of the ITB region and a positive peak in the outer half of the ITB region. While the absolute values of these two peaks are comparable to each other (-1.8 and 1.7 MeV/m^2, respectively) in the ITB at $t = 6.04$ s, the absolute value of these two peaks are different (-1.7 and 0.6 MeV/m^2, respectively) in the ITB at $t = 6.24$ s. Since both the negative and the positive second derivatives always exist in the ITB region, the sign of the curvature of T_i of the ITB (concave or convex) is determined by the second derivative averaged in the ITB region where the first derivative is large ($\rho =$ 0.38-0.76 in this experiment). The curvature asymmetry factor ζ_c is evaluated by the ratio of the averaged second derivative to the averaged absolute value of the second derivative as $\zeta_c = \langle d^2T_i/dr^2\rangle/\langle|d^2T_i/dr^2|\rangle$. The ITB at $t = 6.04$ s with a small positive curvature asymmetry factor ($\zeta_c = 0.08 \pm 0.11$) is called a "weak concave ITB," while the ITB at $t = 6.24$ s with a large negative curvature asymmetry factor ($\zeta_c = -0.43 \pm 0.14$) is called a "strong convex ITB."

The time for the transition from the positive curvature ITB to the negative curvature ITB is 50 ms ($t =$ 5.78–5.83 s) as seen in the time evolution of the T_i gradient at two locations of the ITB region: One is near the shoulder ($\rho = 0.53$), and the other is near the foot point ($\rho = 0.67$)

[Fig. 3(a)]. During the transition phase, the T_i gradient inner half of the ITB region (near the shoulder) decreases, while that of the outer half of the ITB region (near the foot point) increases, and the density profile is almost unchanged. A gradual increase of T_i gradient and a gradual reduction of the ion thermal diffusivity $\chi_i[= -a(Q_e/n_e)/(\partial T_i/\partial \rho)]$ are observed at the early phase of the transition as seen in Figs. 3(a) and 3(c). The error bar of χ_i is mainly attributed to the error bar of the T_i gradient. This gradual transition starts associated with the abrupt drop of the T_i gradient and the abrupt jump of thermal diffusivity at $t = 5.785$ s near the shoulder of the ITB ($\rho = 0.53$). At the later phase of the transition ($t >$ 5.81 s), the rate of increase of T_i exceeds 50 keV/s, and a significant drop in heat flux due to the T_i rise is observed at the outer half of the ITB region as seen in Fig. 3(b). The thermal diffusivity plotted is the ratio of heat flux normalized by density, which is almost unchanged during the transition phase [as seen in Fig. 3(a)] to the T_i gradient.

The radial profile of T_i in the strong convex ITB has a clear foot point, which is due to the discontinuity of transport in space, while the foot point in the plasma with the weak concave ITB is unclear because of the gradual change in transport. The discontinuity of transport at the interface between the L-mode region and the ITB region is evaluated by the sharpness of the drop in the χ_i in space at the interface. As seen in Fig. 4, the radial profiles of χ_i in the weak concave curvature ITB (slice "A") at $t =$ 5.775 s show a gradual decrease with an e-folding length of $34\rho_i$ (5.5 cm), while those in the strong convex ITB (slice "B") at $t = 5.845$ s have a sharp drop with an e-folding length of $15\rho_i$ (2.3 cm). The coherence of the turbulence at the ITB region with a spatial separation of 2.1 cm is measured with a heterodyne reflectometer. As seen in Fig. 4, a significant decrease in the coherence of the turbulence is observed at frequencies below 120 kHz at the time slice B, which suggests a significant change in turbulence between these two ITBs. The change of χ_i in this radial scale is attributed to the penetration of fluctuations. One can compare this penetration distance with the autocorrelation length of fluctuations (on the order of $20\rho_i$ in theory [14] or 1.5 cm as measured in a similar discharge [15]). Our finding clarifies the nature of the transition and the possible penetration length of fluctuations into the improved region. (This stimulates the studies of turbulence spreading [16].)

The discovery reported here has a deep impact on the understanding of the physics of the ITB. The gradient-flux relation that induces the transition of the ITB has been modeled as a cusp catastrophe with a critical point [17–19], as is illustrated in Fig. 5. That is, depending on the sharpness of the turbulence suppression Z, which is related to the penetration of the turbulence, the heat flux is a monotonic function of the gradient or has a slope inversion. The interface between the L-mode region and the improved region is governed by Maxwell's construction rule [17–19]. If the interface is established under the condition of a slope inversion, the discontinuity in the gradient of the slope appears at the interface, and the fluctuations in the L-mode region are repelled from the ITB region [time slice B in Fig. 3(c)]. In contrast, when the interface is formed at the critical point (or beyond it), the discontinuity in the gradient does not exist at the interface and penetration of

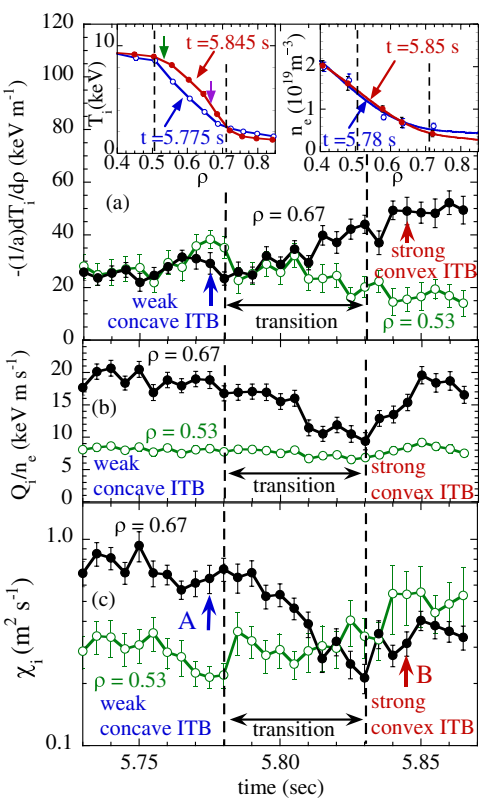

FIG. 3 (color online). Time evolution of the (a) ion temperature gradient, (b) ion heat flux normalized by density, and (c) ion thermal diffusivity at two locations in the ITB region ($\rho = 0.53$ and 0.67). Radial profiles of ion temperature and electron density before and after the transition phase are plotted in (a).

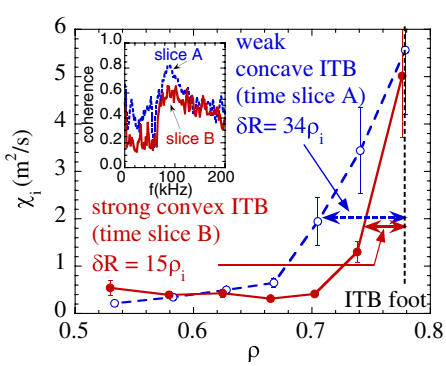

FIG. 4 (color online). Radial profiles of ion thermal diffusivity at $t = 5.775$ s [weak concave curvature ITB: time slice A in Fig. 3(c)] and $t = 5.845$ s [strong convex curvature ITB: time slice B in Fig. 3(c)]. The coherence of the turbulence in the electron diamagnetic direction at the ITB region with a spatial separation of 2.1 cm is also plotted at time slices A and B.

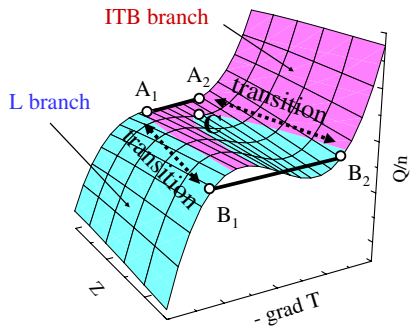

FIG. 5 (color online). Gradient-flux relation that governs the confinement improvement near the foot point of ITB. On the ITB branch, a higher gradient than that of the L branch is allowed for a common heat flux of Q/n. At the interface between the L and ITB regions, the discontinuity of gradient in space (B_1-B_2) can take place. Beyond the critical point (C), there is no discontinuity of gradient (A_1-A_2) across the interface, and the change in T_i becomes smooth. The transition in time between A_1-A_2 and B_1-B_2 can also take place.

fluctuations into the ITB region occurs [time slice A in Fig. 3(c)]. The former case is analogous to the first-order phase transition and the latter to the second-order phase transition. Figure 5 demonstrates that the transition is sharp at one interface of the ITB region, while it is smooth at the other interface. The second derivative of the T_i gradient provides the information of the radial gradient scale length of the anomalous transport coefficient. The change in the turbulence penetration length during this transition in this experiment suggests that the control parameter Z is an indicator to express the magnitude of the turbulence interaction in space, which plays an important role in the nonlocal transport [20–22]. Therefore, the parameter Z is not given by a local variable such as in the conventional models but should be given by integrated variables in space and can be evaluated from the measurements of autocorrelation length. The parameter Z determines the hardness of the bifurcation and controls the sharpness of the interface [at $\rho = 0.65$ in Fig. 1(a)]. This observation stimulates the development of a qualitatively new theoretical modeling of the ITB formation.

In conclusion, discrete eigenprofiles are identified in the "ITB state" and are characterized by the different curvature asymmetry factor. One is a "weak concave ITB," and the other is a "strong convex ITB." The transition between concave and convex ITBs is explained by a cusp catastrophe nonlinear gradient-flux relation model, which is related to the turbulence penetration into the ITB region near the foot points. The time for this transition is 50 ms, which is much smaller than the time scale of the change in the current profile, and is initiated by a small drop in the temperature gradient near the shoulder. The finding of the "concave-convex ITB transition" is important both in plasma physics and in nuclear fusion research. In plasma physics, this observation demonstrates that there is an additional degree of freedom in the ITB radial structure due to the different turbulence states in addition to turbulence suppression due to $E_r \times B$ shearing. In nuclear fusion research, knowledge of the time scale of the concave-convex ITB transition has a significant impact on future research into burning plasmas such as ITER, where stationary operation is required and a large heat pulse due to the rapid change in confinement should be avoided. The time scales of the forward and back transitions between the two ITBs are much faster than the global energy confinement time, which suggests a strong requirement for the fast feedback system of the plasma profile control in order to maintain stationary burning and heat flux to the divertor.

We thank the technical staff for their efforts to support the experiment in JT-60U. This work is partly supported by a Grant-in-aid for Scientific research (No. 18206094) and the Grant-in-Aid for Specially-Promoted Research (No. 16002005) of MEXT Japan.

*Present address: Research Institute for Applied Mechanics, Kyushu University, Kasuga, Fukuoka 816-8580, Japan.

†Present address: Department of Quantum Science and Energy Engineering, Tohoku University, Sendai, Miyagi, 980-8679, Japan.

[1] F. Wagner *et al.*, Phys. Rev. Lett. **49**, 1408 (1982).
[2] R. J. Groebner, K. H. Burrell, and R. P. Seraydarian, Phys. Rev. Lett. **64**, 3015 (1990).
[3] K. Ida *et al.*, Phys. Rev. Lett. **65**, 1364 (1990).
[4] K. Itoh *et al.*, Plasma Phys. Controlled Fusion **38**, 1 (1996).
[5] K. Ida *et al.*, Phys. Rev. Lett. **96**, 125006 (2006).
[6] J. B. Taylor *et al.*, Phys. Plasmas **5**, 3065 (1998).
[7] Y. Koide *et al.*, Phys. Rev. Lett. **72**, 3662 (1994).
[8] F. M. Levinton *et al.*, Phys. Rev. Lett. **75**, 4417 (1995).
[9] E. J. Strait *et al.*, Phys. Rev. Lett. **75**, 4421 (1995).
[10] T. Fujita *et al.*, Phys. Rev. Lett. **78**, 2377 (1997).
[11] Y. Sakamoto *et al.*, Nucl. Fusion **44**, 876 (2004).
[12] Y. Sakamoto *et al.*, Nucl. Fusion **41**, 865 (2001).
[13] K. Ida *et al.*, Rev. Sci. Instrum. **79**, 053506 (2008).
[14] P. H. Diamond *et al.*, Plasma Phys. Controlled Fusion **47**, R35 (2005).
[15] R. Nazikian *et al.*, Phys. Rev. Lett. **94**, 135002 (2005).
[16] X. Garbet *et al.*, Nucl. Fusion **34**, 963 (1994).
[17] K. Itoh *et al.*, Plasma Phys. Controlled Fusion **38**, 1 (1996).
[18] V. B. Lebedev *et al.*, Phys. Plasmas **4**, 1087 (1997).
[19] K. Itoh, S-I. Itoh, and A. Fukuyama, *Transport and Structural Formation in Plasmas* (Institute of Physics Publishing, London, 1999), Chap. 12.
[20] K. W. Gentle *et al.*, Phys. Rev. Lett. **74**, 3620 (1995).
[21] N. Tamura *et al.*, Phys. Plasmas **12**, 110705 (2005).
[22] S. Inagaki *et al.*, Plasma Phys. Controlled Fusion **48**, A251 (2006).